Tumor Biology and Immunology

Cancer Research

Replication Stress Drives Constitutive Activation of the DNA Damage Response and Radioresistance in Glioblastoma Stem-like Cells

Ross D. Carruthers[1], Shafiq U. Ahmed[2], Shaliny Ramachandran[3], Karen Strathdee[1], Kathreena M. Kurian[4], Ann Hedley[5], Natividad Gomez-Roman[1], Gabriela Kalna[5,†], Mathew Neilson[5], Lesley Gilmour[1], Katrina H. Stevenson[1], Ester M. Hammond[3], and Anthony J. Chalmers[1]

Abstract

Glioblastoma (GBM) is a lethal primary brain tumor characterized by treatment resistance and inevitable tumor recurrence, both of which are driven by a subpopulation of GBM cancer stem–like cells (GSC) with tumorigenic and self-renewal properties. Despite having broad implications for understanding GSC phenotype, the determinants of upregulated DNA-damage response (DDR) and subsequent radiation resistance in GSC are unknown and represent a significant barrier to developing effective GBM treatments. In this study, we show that constitutive DDR activation and radiation resistance are driven by high levels of DNA replication stress (RS). $CD133^+$ GSC exhibited reduced DNA replication velocity and a higher frequency of stalled replication forks than $CD133^-$ non-GSC *in vitro*; immunofluorescence studies confirmed these observations in a panel of orthotopic xenografts and human GBM specimens. Exposure of non-GSC to low-level exogenous RS generated radiation resistance *in vitro*, confirming RS as a novel determinant of radiation resistance in tumor cells. GSC exhibited DNA double-strand breaks, which colocalized with "replication factories" and RNA: DNA hybrids. GSC also demonstrated increased expression of long neural genes (>1 Mbp) containing common fragile sites, supporting the hypothesis that replication/transcription collisions are the likely cause of RS in GSC. Targeting RS by combined inhibition of ATR and PARP (CAiPi) provided GSC-specific cytotoxicity and complete abrogation of GSC radiation resistance *in vitro*. These data identify RS as a cancer stem cell–specific target with significant clinical potential.

Significance: These findings shed new light on cancer stem cell biology and reveal novel therapeutics with the potential to improve clinical outcomes by overcoming inherent radioresistance in GBM. *Cancer Res; 78(17); 5060–71. ©2018 AACR.*

Introduction

Despite detailed characterization of the genomic and molecular landscape of glioblastoma (GBM), life expectancy for patients with this aggressive tumor remains extremely poor (1, 2). Standard of care comprises neurosurgical resection followed by treatment with radiotherapy and temozolomide, both of which are DNA-damaging agents (3). Accumulating evidence suggests that the inevitable recurrence of GBM after chemoradiation is driven largely by GBM cancer stem–like cells (GSC), which drive resistance to DNA-damaging therapies through constitutive upregulation of the DNA-damage response (DDR; refs. 4–6). This DDR phenotype has also been reported in cancer stem cells derived from other tumor types (7, 8) and in murine embryonic stem cells (9). Despite a decade of research, however, the underlying cause of DDR upregulation in GSC remains unclear. Although an association with elevated levels of reactive oxygen species (ROS) has been reported (10), other studies have attributed radiation resistance to reduced levels of ROS in cancer stem cells (11).

A consistent feature of the GSC and cancer stem cell DDR phenotype is the upregulation and/or constitutive activation of multiple components of both the DNA repair and cell-cycle checkpoint pathways (4, 12). Previously, we demonstrated the therapeutic relevance of this phenotype by showing that inhibition of both DNA repair and cell-cycle checkpoint function was required to overcome radioresistance (12). Although several other reports have confirmed the radiosensitizing potential of DDR inhibition at the preclinical level (10, 13), progression to the clinic has been frustratingly slow. The aim of this study was to elucidate the mechanisms underlying constitutive DDR activation in GSC and use this knowledge to identify new therapeutic strategies for this cancer of unmet need. Our approach was informed by previous studies describing elevated levels of DNA replication

[1]Institute of Cancer Sciences, Wolfson Wohl Cancer Research Centre, University of Glasgow, Glasgow, United Kingdom. [2]School of Pharmacy and Pharmaceutical Sciences, Faculty of Health Sciences and Wellbeing, University of Sunderland, Sunderland, United Kingdom. [3]Cancer Research UK/MRC Oxford Institute for Radiation Oncology, Department of Oncology, University of Oxford, Oxford, United Kingdom. [4]Department of Neuropathology, Brain Tumour Research Group, Frenchay Hospital, North Bristol NHS Trust Bristol, Bristol, United Kingdom. [5]Cancer Research UK Beatson Institute, Glasgow, United Kingdom.

Note: Supplementary data for this article are available at Cancer Research Online (http://cancerres.aacrjournals.org/).

†Deceased.

R.D. Carruthers and S.U. Ahmed contributed equally to this article.

Corresponding Author: Ross D. Carruthers, Institute of Cancer Sciences, Wolfson Wohl Cancer Research Centre, University of Glasgow, Gascube Estate, Glasgow G61 1QH, UK. Phone: 141-211-3000; Fax: 141-3301-4890; E-mail: ross.carruthers@glasgow.ac.uk

doi: 10.1158/0008-5472.CAN-18-0569

stress (RS) in glioma specimens, particularly GBM (14), and by emerging evidence that RS can activate a broader spectrum of DDR proteins than previously thought (15). RS can be defined as inefficient DNA replication that causes replication forks to progress slowly or stall, and may be caused by a wide variety of cellular and environmental factors (16, 17). Because RS can have adverse consequences, including permanent DNA damage and genomic instability, it evokes a spectrum of cellular responses that act to stabilize stalled forks and reduce the risk of fork collapse and consequent DNA damage. Extensive overlap between the cellular responses to RS and radiation-induced DNA damage supports the hypothesis that constitutive RS might be responsible for radiation resistance.

A further question is whether GSC arise from neural progenitor cells, or are the product of dedifferentiation of malignant glioma cells (18). Embedded within this controversy is the related question of whether neural progenitor cells are the cell of origin of GBM (19). The recently published observation that neural progenitor cells are prone to acquisition of DNA double-strand breaks (DSB) at specific chromosomal sites as a consequence of RS induced by transcription of long neural genes (20) strengthens the rationale for exploring RS in GSC with a view to exploring a potential phenotypic link between these two cell populations.

In this study, we demonstrate that GSC exhibit constitutively elevated RS both *in vitro* and *in vivo*, and that S-phase GSC exhibit increased levels of DSB, which arise at DNA "replication factories." We show that exposure to exogenous RS generates significant radiation resistance in relatively radiosensitive non-GSC glioma cells. We provide evidence to support the hypothesis that RS and consequent activation of the DDR is associated with marked overexpression of very long genes, of which the most profoundly upregulated are the long neural genes previously shown to harbor DSB in neural stem cells (20). Finally, we show that targeting the RS response through combined ataxia telangiectasia- and rad3-related protein (ATR) inhibition and poly (ADP-ribose) polymerase (PARP) inhibition (CAiPi) is an effective approach to overcoming the intrinsic radiation resistance of GSC.

Materials and Methods

Derivation and maintenance of primary GBM cell lines

Primary GBM cell lines E2, G7, R10, R15, R24, R9, and S2 were derived from resected tumors and maintained as described previously (12, 21), approved by the local regional Ethics Committee (LREC ref 04/Q0108/60) in compliance with the UK Human Tissue Act 2004 (HTA License ref 12315). Tumorigenicity of paired GSC and differentiated GBM cell lines has been described previously (summarized in Supplementary Table S1; refs. 12, 21). Cell lines were utilized for 20 passages from thaw prior to being discarded and were tested for the presence of mycoplasma using the Lonza MycoAlert (LT07-318) assay on a 3-monthly basis.

Immunohistochemistry/immunofluorescence on tissue sections

Immunofluorescence microscopy on paraffin-embedded sections was carried out as described previously (22). Following antigen retrieval, sections were incubated sequentially with primary and secondary antibodies (Supplementary Tables S2 and S3). Immunofluorescence images were acquired as Z stacks with a Zeiss 780 confocal microscope and processed using maximum intensity projection method, where individual nuclei were selected and quantified for mean fluorescent intensity (MFI) values using ImageJ. Sox2 high and low values were characterized as being above and below the median Sox2 MFI value in the whole imaged cell population, respectively, with the MFI of RPA32 being compared between the two groups. A minimum of 150 (range, 150–700) nuclei per sample were quantified from 6 to 12 63× magnification fields. Nonfluorescent immunohistochemistry slides were imaged using a Leica Slidepath system.

Clonogenic and neurosphere assays

Clonogenic survival assays were performed as described previously (12, 23). Cells were treated with DDR inhibitors or DMSO for 1 hour followed by mock or 1 to 5 Gy irradiation. Cells were then incubated for a further 24 hours followed by replacement with fresh media without DDR inhibitor. Cell cultures were incubated with aphidicolin (Sigma) 0.05 μmol/L (or DMSO) for 72 hours then plated in media with no added aphidicolin and irradiated 1 hour after plating. Colonies were fixed in methanol after 2 to 3 weeks, stained with crystal violet, and counted manually. Clonogenic survival data were fitted using a linear quadratic model and dose-modifying factors (DMF) of 0.37 and SER 0.37 were calculated from the fitted curve. Significance between survival curves was assessed by two-way ANOVA.

For neurosphere assay, 10 GSC were seeded into each well of a 96-well plate in 100 μL medium containing 1 μmol/L olaparib and/or 5 μmol/L VE821 or DMSO control for 48 hours or irradiated with 2 Gy ionizing irradiation, followed by the addition of 150 μL of fresh media per well. Neurospheres were manually counted under ×5 magnification after 3 to 4 weeks.

Flow cytometry and cell viability

$CD133^+$ and $CD133^-$ populations were isolated using a FACSAria fusion platform following labeling with CD133 phycoerythrin (PE)-conjugated antibody. Live cells were gated (Supplementary Fig. S1A), and sorted populations were grown in identical stem cell culture media for 3 to 7 days prior to harvesting.

Levels of ROS were measured using the dichlorodihydrofluorescein diacetate (DCFDHA) OxiSelect *In Vitro* ROS Assay Kit according to the manufacturer's protocol (Cell Bio Labs Inc.). Briefly, bulk and GSC were harvested and incubated in PBS containing DCFDHA at 37°C for 20 minutes. Samples were washed twice in PBS followed by flow cytometry analysis of live cells. Dead cells were excluded using DAPI.

Cell-cycle analysis using BrdUrd was carried out as described previously (12). Briefly, bulk and GSC were incubated with 10 μmol/L BrdUrd for 35 minutes. Cells were washed in PBS and fixed in 70% ethanol. Samples were costained with anti-BrdUrd-FITC antibody (BD Bioscience) and propidium iodide. Flow cytometry data were collected using FACSVerse (BD Biosciences) following doublet discrimination and analyzed using FlowJo software (Tristar).

Cell viability was carried out using CellTiter-Glo according to the manufacturer's protocol (Promega). Briefly, bulk cells and GSC were plated out in 96-well plates and treated with olaparib (1 μmol/L) and VE821 (1, 3, or 5 μmol/L) for 24 hours or 6 days, replaced with fresh media, and cultured for a further 5 days followed by detection of luminescence (Promega GLOMAX).

In vitro immunofluorescence

Paired bulk and GSC were plated on coverslips coated with Matrigel. For BrdUrd studies, subconfluent paired bulk and/or GSC were cultured on coverslips and pulse labeled with 10 μmol/

L of BrdUrd for 30 minutes followed by fixation in 4% formaldehyde. Immunofluorescent visualization of RPA and pATM s1981 required removal of nonchromatin bound nuclear protein using an extraction buffer (24). Coverslips were washed in PBS and denatured in 2 mol/L HCl followed by immunostaining with anti-BrdUrd and γH2AX antibodies. For DDR inhibition studies, subconfluent cells were incubated with olaparib and/or VE821 for 24 hours and fixed in 4% formaldehyde. Cells were incubated with anti-γH2AX, BrdUrd, RPA 32, and 53BP1 antibodies overnight at 4°C followed by incubation with secondary conjugated antibodies (Supplementary Tables S2 and S3). Nuclei were counterstained with Vectashield mount containing DAPI. Z-stack images were acquired under identical parameters using Zeiss LSM 780 confocal microscope and analyzed using Zen 2012 (Zeiss). Colocalization was carried out using Zen Black software (Zeiss) from Z-stack images obtained at 40× magnification on a Zeiss 780 confocal microscope. Colocalization coefficients defined as the relative number of BrdUrd pixels that colocalize with γH2AX pixels or relative number of γH2AX pixels that colocalize with S9.6 pixels; value range 0–1, where 0 denotes no colocalization and 1 represents all pixels colocalized and expressed as a percentage. Fifty to 75 BrdUrd positive or 50 to 100 drug-treated cells were analyzed, and each experiment was repeated at least three times.

DNA fiber assays

DNA fiber assays were performed as described previously (15). Briefly, cultured cells were incubated for 20 minutes with media containing CIdU (25 μmol/L) followed by PBS wash and incubation with media containing IdU (250 μmol/L). Cell suspensions were pipetted onto glass microscopy slides and lysed. Slides were raised to an angle of 30° in order to stretch DNA fibers along the slide. Immunostaining was then performed. CIdU was detected using anti-BrdUrd (rat) primary antibody (Abcam ab6326 1:400) and anti-rat alexa fluorophore 555 (Invitrogen A21434 1:500) secondary. IdU was detected using anti BrdUrd (mouse) primary antibody (BD 347580 1:500) and anti-mouse alexa fluorophore 488 (Invitrogen A11017 1:500).

Drug treatment and radiation

ATR inhibitor VE821 (Vertex Pharmaceuticals) and PARP inhibitor olaparib (Selleckchem) were dissolved in DMSO and used at concentrations stated. A concentration of 5 μmol/L VE821 was found to be sufficient to inhibit phosphorylation of Chk1s345 following 5 Gy radiation (Supplementary Fig. S1B). An XStrahl RS225 cabinet at room temperature with 195 kV/15 mA X-rays producing a dose rate of 1.6 Gy per minute was utilized for *in vitro* radiation studies. For UV studies, media were removed, and cells were irradiated with 10 per JM^2 UV (Stratalinker, Stratagene).

Western blotting

Western blotting was carried out as described previously (23).

RNA sequencing and bioinformatics

Total RNA was extracted from 7 paired bulk and GSC followed by generation of TruSeq Stranded mRNA library. Samples were run on four V3 flow cells with seven indexes per lane and sequenced on an Illumina HiSeq 2000 to generate 30 to 45 M 100 paired-end reads (Supplementary Materials and Methods). RNA-sequencing data files were quality checked using FastQC and FastQ-Screen (www.bioinformatics.babraham.ac.uk). RNA-sequencing reads were aligned to the GRCh37 version of the human genome (25) using Tophat2 version 2.0.10 (26) with Bowtie version 2.1.0 (27). Relative expression levels were determined and statistically analyzed by a combination of HTSeq and the R 3.0.2 environment, utilizing packages from the Bioconductor data analysis suite and differential gene expression analysis based on the negative binomial distribution using the DESeq package (28).

Statistical analyses

All experiments were repeated and data points were reported as mean ± SEM. Correlation of Sox2- and RPA32-integrated density was performed using Spearman ranks due to nonnormal distribution of these variables. Two-way ANOVA was utilized in analyses of clonogenic survival curves. Means were compared by unpaired Student *t* test. Medians were compared by Mann–Whitney *U* test. Statistical analysis and graphs were produced using Minitab 16 and GraphPad Prism 6.

Results

Radioresistant GSC demonstrate upregulation of DNA RS response markers

We previously characterized constitutive DDR activation and associated radioresistance of GSC in a panel of primary GBM cell lines propagated as paired GSC-enriched ("GSC") and GSC-depleted ("bulk") cultures (12, 23, 29). Increased expression of the GSC markers Nestin and Sox2 along with constitutive upregulation and activation of the DDR proteins Chk1 and ATR was confirmed in GSC cultures by Western blot (Fig. 1A). Using a DCFHDA assay, no significant differences in baseline ROS levels between GSC and tumor bulk cultures were observed (Fig. 1B), so alternative mechanisms to explain the upregulated DDR in GSC were investigated. The consistent pattern of robust upregulation of phosphorylated ATR (Ser428) and phosphorylated CHK1 (Ser345) in GSC cultures (Fig. 1A) led us to hypothesize that GSC populations might exhibit high levels of RS. Replication protein A (RPA) binds single-stranded DNA (ssDNA) adjacent to collapsed or stalled replication forks and is necessary for the activation of ATR kinase in the cellular response to RS (30). Validation of the RS phenotype was therefore sought by probing for phosphorylation of RPA subunit 32 (RPA32) at Ser4 and Ser8, which is a specific marker of RS (31). Although phospho-RPA32 (Ser4/8) levels were not detectable by Western blot in asynchronous undamaged cells, exacerbation of RS by low doses of UV radiation (10 per Jm^2) elicited markedly greater phosphorylation of RPA32 in GSC than in paired tumor bulk populations (Fig. 1C). Pulse labeling with BrdUrd revealed that RPA immunofluorescence intensity was significantly higher in S-phase GSC than in tumor bulk cells in E2 and G7 cell lines; a trend toward higher intensity in R10 GSC narrowly failed to reach statistical significance (Fig. 1D and E). Although γH2AX foci are markers of DNA DSB, diffuse nuclear staining is also observed under conditions of RS (Supplementary Fig. S1C; refs. 32, 33) with overall nuclear MFI correlating with levels of RS. In E2, G7, and R10 cultures, S-phase GSC demonstrated significantly higher γH2AX diffuse MFI than corresponding tumor bulk cells, providing further evidence of elevated RS (Fig. 1D and E).

Exogenous RS can generate a radiation resistance phenotype in non-GSC

The hypothesis that exogenous RS could stimulate the DDR and thus enhance radioresistance was tested by incubating bulk

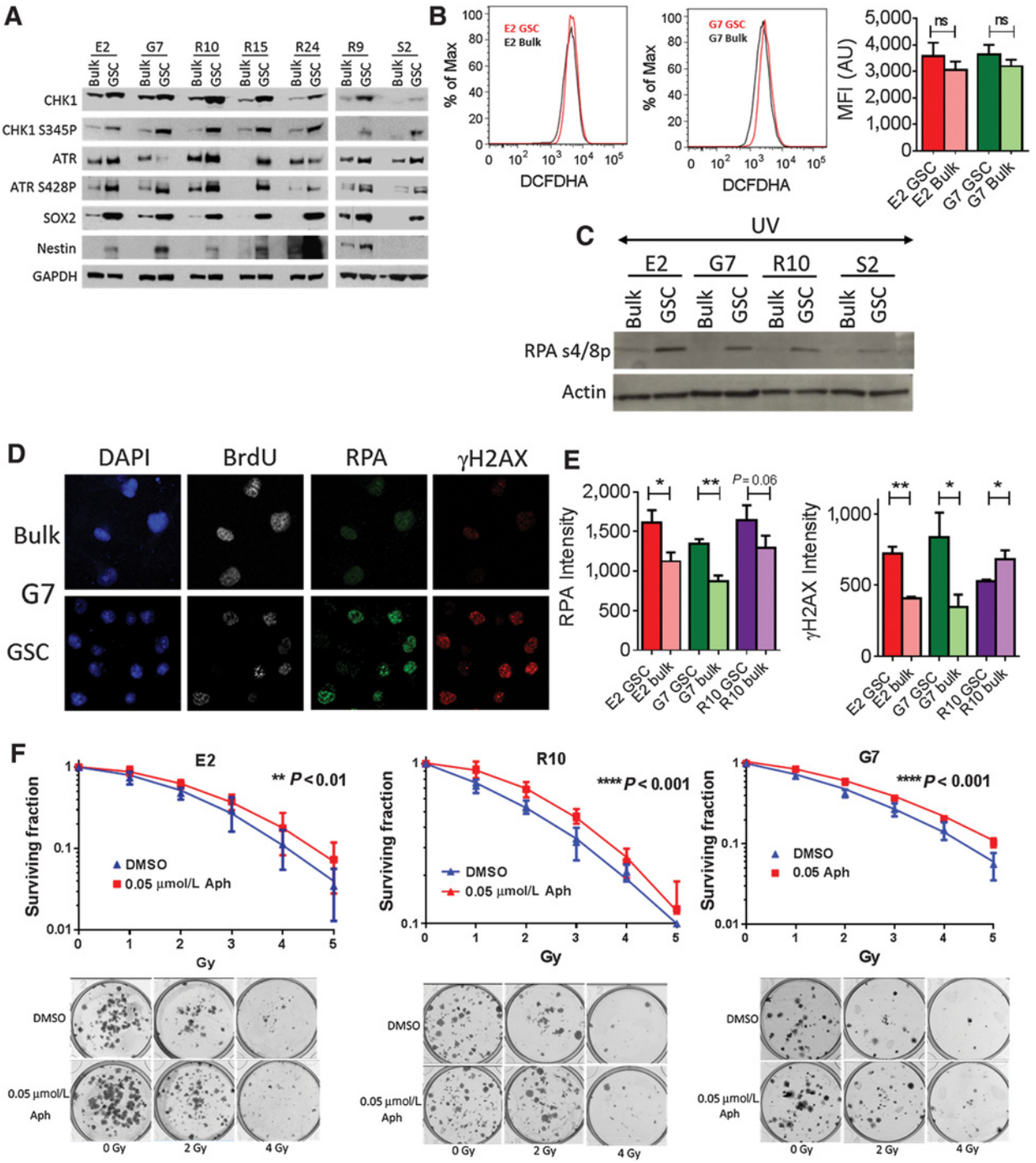

Figure 1.

Radioresistant GSC demonstrate upregulation of DNA RS response markers, and exogenous RS generates radiation resistance in non-GSC. **A,** Western blot analysis of RS response and GSC markers in a panel of paired GSC and tumor bulk primary GBM cultures. GAPDH, loading control. **B,** Flow cytometry plots showing baseline levels of ROS via quantification of DCFHDA MFI in GSC and tumor bulk cultures (mean ± SEM, $n = 3$; unpaired t test; NS, nonsignificant). **C,** Western blot analysis of phospho-RPA32 (Ser4/8) expression in a panel of paired GSC and tumor bulk cells following UV-mediated activation of RS (10 per Jm^2). **D,** Immunofluorescence images showing γH2AX and RPA32 staining in BrdUrd-positive G7 GSC and tumor bulk cells under basal conditions. Nuclei were counterstained with DAPI. **E,** Quantification of γH2AX and RPA32 MFI in E2, G7, and R10 GSC and tumor bulk cells (mean ± SEM, $n = 3$; *, $P < 0.05$; **, $P < 0.01$; unpaired t test). **F,** Clonogenic survival of E2, R10, and G7 tumor bulk cell lines treated with radiation alone (blue line) and following incubation with 0.05 μmol/L aphidicolin (red line) for 72 hours prior to irradiation (mean ± SEM, $n = 3$; **, $P < 0.01$; ****, $P < 0.001$ by two-way ANOVA). Representative images of colonies formed following 0, 2, and 4 Gy are shown.

cultures of E2, G7, and R10, which are radiosensitive relative to E2, G7, and R10 GSC cultures (12, 23), with 0.05 μmol/L aphidicolin for 72 hours prior to irradiation. This low concentration of aphidicolin is known to slow DNA replication fork speed and generate RNA:DNA hybrids, leading to RS and DDR activation (34, 35) but was not sufficient to induce S-phase arrest or affect plating efficiency in the absence of radiation in these experiments (Supplementary Fig. S2A, S2i, S2ii). Exposure to 0.05 μmol/L aphidicolin also generated an excess of pATM s1981 foci in exposed cell cultures versus controls, demonstrating the activation of DDR DNA DSB pathways by an exogenous source of RS (Supplementary Fig. S2A, S2iii). Importantly, all bulk cell lines examined exhibited a significant increase in radioresistance after exposure to low dose aphidicolin, confirming that exogenously induced RS can generate measurable radiation resistance *in vitro* (Fig. 1F). Survival curves for DMSO- versus aphidicolin-treated irradiated cells were significantly different in all cell lines and DMFs at 0.37 survival (and 95% confidence intervals) were 0.83 (0.76–0.9), 0.80 (0.68–0.92), 0.82 (0.52–1.12) in the E2, G7, and R10 cell lines, respectively (Supplementary Fig. S2A, S2iv). Surviving fractions at 2 Gy (SF2 Gy) are plotted in Supplementary Fig. S2A, S2v.

Replicating GSC show altered cell-cycle progression and increased RS *in vitro*

Cell-cycle studies demonstrated significantly higher proportions of S-phase cells in GSC than in tumor bulk populations (Fig. 2A), despite GSC cultures having similar proliferation rates to tumor bulk cultures as shown in previous work (12), indicating that GSC have a prolonged S-phase duration. A likely explanation is that GSC have slower DNA replication velocity than tumor bulk populations because of elevated RS.

We confirmed elevated RS levels in GSC using the gold-standard DNA fiber assay (Fig. 2B–D) in which immunofluorescent staining of sequentially incorporated nucleotide analogues CIdU (red) and IdU (green) facilitates visualization of DNA replication structures and direct measurement of DNA replication velocities (Fig. 2B). GSC cultures exhibited significantly slower DNA replication velocities than matched tumor bulk populations (Fig. 2B), as well as higher percentages of stalled replication forks and fewer ongoing forks, all of which are consistent with increased RS (Fig. 2C). GSC cultures also showed a consistent trend toward a higher percentage of new origin replication structures; however, this only reached significance in the G7 cell line. To exclude the possibility that these observations were caused by GSC culture conditions, we repeated the assay utilizing cell populations, which were sorted using the putative GSC markers CD133 and CD15. $CD133^+$ (GSC) and $CD133^-$ (non-GSC) sorted E2 cells when cultured in identical conditions for several passages, maintained GSC and non-GSC (bulk) phenotypes respectively. Importantly, $CD133^+$ cells exhibited reduced replication velocity, increased frequency of stalled forks and fewer ongoing forks than their $CD133^-$ counterparts. Studies in the G7 cell line examining $CD15^+$ GSC and $CD15^-$ non-GSC cell sorted populations confirmed these findings. Further quantitative analyses of bidirectional fork replication structures in the E2 cell line supported our hypothesis. Bidirectional forks represent DNA replication arising from a single origin and proceeding in two opposing directions. In the absence of RS both forks proceed at the same velocity, leading to symmetrical green IdU tracks flanking a central red CIdU origin (Fig. 2D), i.e., IdU1/IdU2 $\approx$ 1. E2 GSC exhibited a greater proportion of asymmetric versus symmetric bidirectional replication forks (Fig. 2D) in comparison with E2 bulk cultures (asymmetry defined as >33% difference in length between bidirectional elongating IdU fibers, i.e., IdU1/IdU2 $\geq$ 1.33; ref. 36). This effect was also observed in E2 $CD133^+$ versus $CD133^-$ sorted cell populations (Fig. 2D). Linear regression of long versus short track length showed significantly different gradient values for E2 GSC versus bulk cells and for E2 $CD133^+$ versus $CD133^-$ cells (Fig. 2D). Taken together, our results show that RS in GSC is associated with reduced DNA replication velocity and higher rates of fork stalling.

GSC exhibit increased numbers of γH2AX foci, which colocalize with replication factories and RNA:DNA hybrids

Reduced DNA fork speed and other evidence of elevated RS led us to hypothesize that S-phase GSC would harbor elevated numbers of DNA DSBs as a direct consequence of perturbed DNA replication. Consistent with this hypothesis, S-phase GSC identified by BrdUrd incorporation had significantly more 53BP1 nuclear foci than tumor bulk cells (Fig. 3A). γH2AX foci were also more numerous in S-phase GSC than in tumor bulk cells (Fig. 3B). Furthermore, in S-phase GSC cultures, γH2AX foci colocalized with areas of intense BrdUrd staining, which represent concentrations of replication forks and their associated DNA replication machinery and have been described as "replication factories" (37). Colocalization of γH2AX and BrdUrd foci was significantly higher in GSC than tumor bulk cells (Fig. 3C), confirming formation of DNA DSBs during aberrant DNA synthesis and providing a likely explanation for constitutive DDR activation in GSC.

To explore potential mechanisms responsible for elevated RS in GSC, we analyzed changes in global gene expression profile between paired GSC and tumor bulk cells derived from 7 primary GBM cell lines using high-throughput RNA sequencing. We first investigated if genes associated with DNA replication and/or the cellular response to RS were responsible for elevated RS in GSC. For this purpose, expression levels of genes encoding proteins known to be enriched on nascent DNA during unperturbed replication ("replication machinery" genes) and under conditions of RS induced by exposure to hydroxyurea ("HU stalled forks" genes) from previously published lists were examined in GSC and bulk cell populations (35). Overall, no significant differences in expression of "replication machinery" or "HU stalled fork" genes were observed between GSC and tumor bulk cells (Supplementary Fig. S2B S2i, S2ii). Indeed only 2 of 82 transcribed "replication machinery" genes and 4 of 131 transcribed "HU stalled fork" genes showed greater than 2.5-fold differential expression between GSC and bulk cells. From these data, we concluded that altered expression of genes associated with nascent DNA was unlikely to be responsible for elevated RS in GSC.

Given that aphidicolin could generate radiation resistance in our non-GSC primary GBM cultures (Fig. 1F) and is known to generate RNA:DNA hybrids, we next investigated the hypothesis that the RS phenotype and its accompanying DDR might be associated with replication–transcription machinery collisions with subsequent common fragile site (CFS) breakage. CFS are chromosomal loci with an increased tendency to develop DNA DSBs under conditions of RS and occur preferentially within very large genes (VLG) that are transcriptionally active (35, 38, 39). RNA-sequencing data revealed that 14 of 73 VLGs (>850 Kbp in length) demonstrated a 2.5-fold or greater expression in GSC

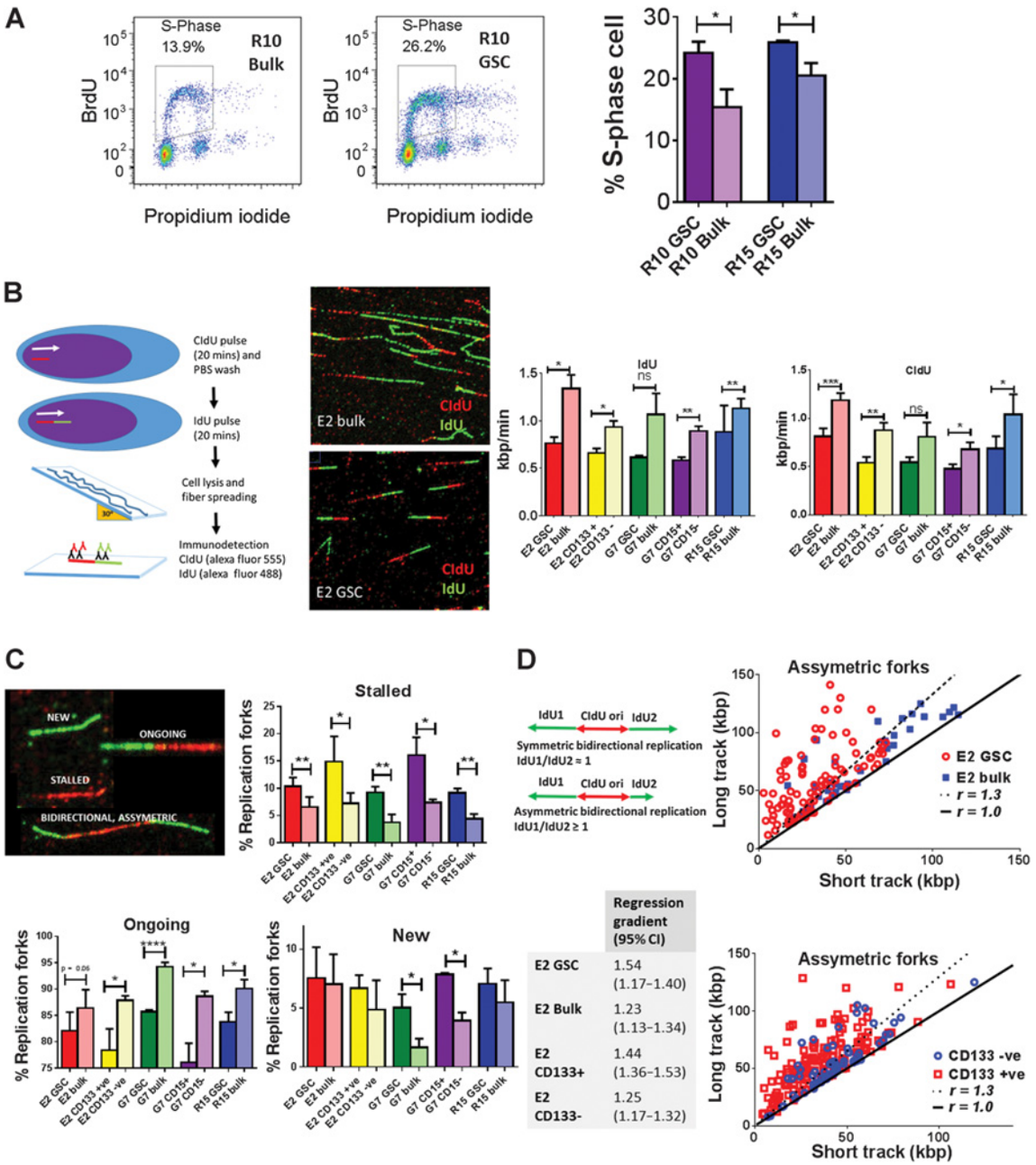

Figure 2.

Replicating GSC show altered cell-cycle phase progression and enhanced RS *in vitro.* **A,** Representative flow cytometry plots and analysis of S-phase populations in R10 and R15 GSC and tumor bulk cells by quantification of BrdUrd incorporation under basal conditions (mean ± SEM, $n = 3$; *, $P < 0.05$; unpaired t test). **B,** Schematic of DNA fiber assay. Cells were incubated sequentially with CldU (red) then IdU (green), followed by lysis and spreading. Representative immunofluorescent images of DNA fibers obtained from E2 GSC and bulk cells. Bar charts summarize quantification of IdU and CldU incorporation rates (replication velocities) in GSC and tumor bulk cells in E2, G7, and R15 cell lines and in E2 CD133$^+$ and CD133$^-$ populations and G7 CD15$^+$ and CD15$^-$ populations (mean ± SEM, $n = 3$; ≥ 500 ongoing replication forks analyzed per data point; *, $P < 0.05$; unpaired t test). **C,** Representative immunofluorescent images showing "new," "ongoing," "stalled," and "bidirectional" replication fork structures following sequential pulse labeling with CldU (red) and IdU (green) in E2 GSC cultures. Bar charts summarize quantification of stalled, ongoing, and new replication forks (as a percentage of total number of replication structures identified) in paired GSC and bulk cultures of E2, R15, and G7 cell lines and also in E2 CD133$^+$ and CD133$^-$ and G7 CD15$^+$ and CD15$^-$ sorted populations. Mean ± SEM; unpaired t test; with approximately 1,800 replication forks identified and counted for each cell line, $n \geq 3$. **D,** Schematic showing symmetric and asymmetric bidirectional DNA replication fork structures observed in DNA fiber assay. Analysis of bidirectional replication fork ratio in E2 GSC and bulk cultures and also in E2 CD133$^+$ and CD133$^-$ sorted populations. Each point represents an individual bidirectional replication fork, with longer IdU (green) track plotted on the y axis versus shorter IdU track on the x axis. Plotted solid black line represents a ratio of 1 (i.e., no asymmetry), while plotted dotted black line represents a ratio of ≥1.33 (i.e., asymmetry). The table shows gradient of best-fit linear regression lines (95% CI) of long IdU versus short IdU tracks in paired E2 GSC and bulk and in E2 CD133$^+$ and CD133$^-$ populations. *, $P < 0.05$; **, $P \leq 0.01$, ***, $P \leq 0.001$, ****, $P \leq 0.0001$; ns, nonsignificant.

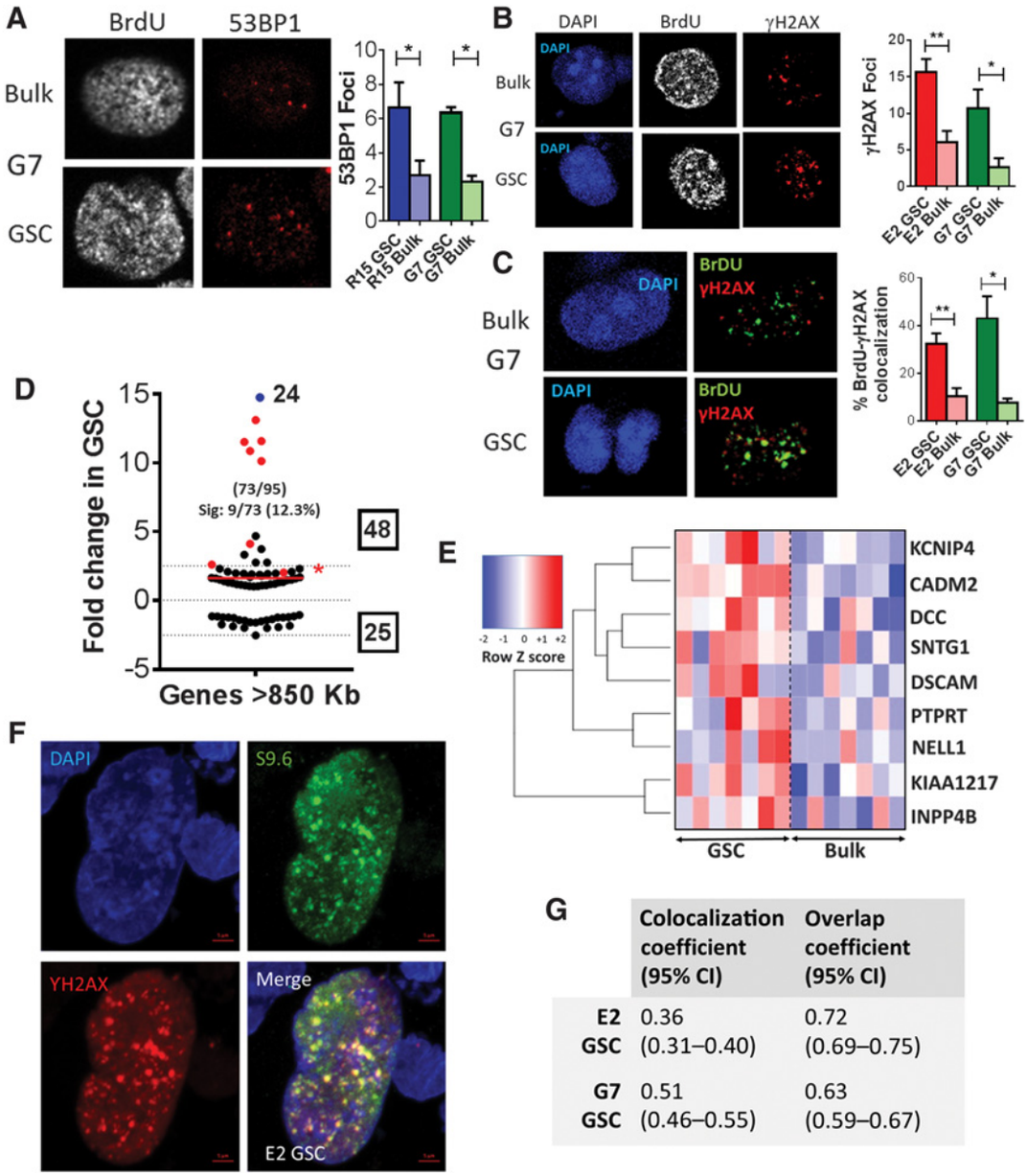

G

	Colocalization coefficient (95% CI)	Overlap coefficient (95% CI)
E2 GSC	0.36 (0.31–0.40)	0.72 (0.69–0.75)
G7 GSC	0.51 (0.46–0.55)	0.63 (0.59–0.67)

Figure 3.

GSC demonstrate increased numbers of γH2AX foci, which colocalize with replication factories and RNA:DNA hybrids. **A** and **B,** Representative immunofluorescence images of G7 GSC and tumor bulk cells showing 53BP1 (**A**) and γH2AX (**B**) foci in BrdUrd-positive cells under basal conditions, with quantification of 53BP1 (**A**) and γH2AX (**B**) foci per S-phase nucleus in G7 and E2 GSC and tumor bulk cells (mean ± SEM, $n = 3$; *, $P < 0.05$; **, $P < 0.01$). **C,** Representative images demonstrating colocalization of γH2AX foci with BrdUrd replication factories (BrdUrd foci) in G7 GSC and tumor bulk cells. Percentages of BrdUrd-positive replication factories colocalizing with γH2AX foci are quantified in E2 and G7 GSC and tumor bulk cells (mean ± SEM, $n = 3$; *, $P < 0.05$; **, $P < 0.01$; unpaired t test). **D,** Mean fold change in the expression of genes across 7 GSC cultures compared with the paired tumor bulk cells associated with genes >850 kb in length. Numbers of genes identified from the RNA-sequencing data and total numbers of genes in the published gene data set are shown in brackets, and total numbers of upregulated and downregulated genes are indicated in boxes. The numbers and percentages of significantly altered ("Sig") genes in each data set are shown, and these genes are highlighted in red. Gene shown in blue was upregulated 24-fold. Mean fold changes across all genes are shown by red lines. Genes >850 bp in length are significantly upregulated in GSC compared with paired tumor bulk population across 7 GBM cell lines (one sample t test; *, $P < 0.05$; NS, nonsignificant). **E,** Heatmap illustrating fold changes in expression of the 9 significantly upregulated genes >850 bp across 7 paired cell lines. **F,** Representative image of immunofluorescent staining for RNA:DNA hybrids using S9.6 antibody and γH2AX in E2 GSC. **G,** Table of colocalization and overlap coefficients (95% CIs) for γH2AX versus S9.6 immunofluorescence in E2 and G7 GSC.

relative to tumor bulk cells (Fig. 3D), and that 9 of these genes were significantly overexpressed compared with paired bulk populations across all 7 cell lines (Fig. 3D). If VLGs are defined more stringently as being greater than 1 Mbp in length, the association remained significant: expression of 5 of 31 genes >1 Mbp was >2.5-fold greater in GSC than in bulk cells, of which 3 were significantly overexpressed across all 7 cell lines (Fig. 3E). These include: deleted in colorectal carcinoma (DCC), cell adhesion molecule 2 (CADM2), and protein tyrosine phosphatase receptor type T (PTPRT), which have been shown to play important roles in the regulation of neurological development, axon guidance, and synapse formation (40–42). In order to investigate the contribution of replication–transcription collisions to DNA DSB generation in GSC, immunofluorescent staining for RNA:DNA hybrids (S9.6) and γH2AX was carried out and colocalization studies were performed. These data demonstrated significant colocalization and overlap of γH2AX foci with areas of intense S9.6 immunofluorescence in E2 and G7 GSC populations, suggesting a prominent role for replication–transcription collisions as a source of DNA DSBs in GSC (Fig. 3F and G). Consistent with these findings, a recent study by Wei and colleagues demonstrated that long neural genes harbor recurrent DNA break clusters in neural stem/progenitor cells (20). In addition, a further study has identified intragenic DNA origin firing in highly transcribed genes with consequent replication–transcription collisions as a mechanism for oncogenic RS (43). Although much debated, neural progenitor cells have been proposed as a cell of origin for GBM (44). Therefore, the description of RS induced DNA DSB formation in transcriptionally active long neural genes in neural progenitor cells and the role of intragenic origins in generating oncogenic RS are highly relevant to our own data in GSC. We propose that replication–transcription collisions due to active transcription of long neural genes in GSC is responsible for the elevated RS in GSC, resulting in generation of DNA DSBs, constitutive DDR activation and consequent therapeutic resistance.

GSC show enhanced RS in murine intracranial orthotopic xenografts and in human GBM tumor samples

Having observed compelling evidence of increased RS in GSC *in vitro*, we investigated whether this phenotype was also present *in vivo*. Dual immunofluorescent staining for RPA32 and the putative GSC marker Sox2 was undertaken in sections of orthotopic xenograft tumors derived from $CD133^+$ E2 GSC, which generate highly invasive, diffuse tumors and in tumors derived from G7 GSC, which form a tumor mass with an invasive front typical of human GBM (Fig. 4A and B and Supplementary Fig. S3A–S3E). Our data showed a higher MFI of RPA32 staining in high (defined as greater than median) Sox2 expressing cells relative to low (less than median) Sox 2 expressing cells, consistent with the presence of elevated RS levels in the GSC subpopulation. MFI values of Sox2 and RPA32 also showed a significant positive correlation (Fig. 4A and B). Further studies in G7 GSC and $CD133^+$ E2 xenografts confirmed increased RS in GSC, utilizing alternative GSC (Olig2) and RS (PARP-1) markers (Supplementary Fig. S4 S4A–S4C).

Further immunohistochemical staining for HLA, RPA32, Ki67, and γH2AX was performed in sections of xenografts derived from $CD133^+$ E2 GSC, in which the majority of HLA expressing tumor cells stained strongly positive for the GSC marker Sox2 (Supplementary Fig. S3A and S3D). Tumor sections also exhibited widespread positivity for Ki67, RPA32, and γH2AX nuclear staining, indicating high levels of RS in replicating GSC *in vivo*.

To confirm the clinical relevance of these observations, dual immunofluorescence staining for Sox2 and RPA32 was performed in human tumor sections from 4 patients with GBM (Fig. 4C and Supplementary Fig. S5A–S5D). Consistent with our earlier xenograft studies (Fig. 4A and B), MFI of RPA32 was significantly higher in cell populations that exhibited greater than median MFI of Sox2 (Fig. 4C). This observation was reproduced using Olig2 as a GSC marker (Supplementary Fig. S5D). RPA32 and Sox2 expression also showed significant positive correlation in all tumors examined (Supplementary Fig. S5A–S5C).

Inhibition of the RS response in GSC reduces neurosphere formation, generates DNA DSBs, and abrogates radiation resistance

Our data indicate that constitutive RS represents a promising, GSC-specific therapeutic target in GBM, which is a cancer of unmet need. To validate this concept, we used olaparib, a small-molecule inhibitor of poly (ADP-ribose) polymerase (PARP) currently in clinical trials for GBM, and VE821, a potent and specific inhibitor of ATR (45), to target key elements of the DDR and RS responses. PARP1 facilitates restart of stalled replication forks (46) while ATR has a key role in enabling cells to tolerate RS via activation of cell-cycle checkpoints, inhibition of global origin firing and stabilization of stalled replication forks. Inhibition of ATR (5 μmol/L VE821) significantly inhibited neurosphere formation in all three GSC populations tested whereas inhibition of PARP (1 μmol/L olaparib) had little or no effect (Fig. 5A). However, addition of olaparib to VE821 (combined ATR inhibition and PARP inhibition; "CAiPi") yielded significant, supra-additive inhibition of neurosphere formation, which is a fundamental property of GSC that requires proliferation and self-renewal. Because tumor bulk cultures do not form neurospheres, cell viability assays were undertaken to enable comparison of the effects of CAiPi on paired GSC and tumor bulk cultures. Consistent with our hypothesis that RS is an integral and targetable characteristic of GSC, these populations were significantly more sensitive to CAiPi than tumor bulk cells (Fig. 5B). Addition of PARPi to GSC or bulk cultures did not affect DNA replication velocities at the clinically relevant concentrations examined, whereas addition of ATRi or CAiPi reduced replication velocities in both GSC and bulk (Fig. 5C). Further mechanistic studies in E2 cells showed increased induction of γH2AX foci and micronuclei (Fig. 5C) in GSC by CAiPi, supporting the concept that higher basal RS in GSC renders them particularly vulnerable to increased DNA damage and consequent cell death when subjected to inhibition of the DDR. Furthermore, and of profound clinical relevance, clonogenic survival assays revealed that CAiPi completely abrogated the radioresistance of GSC (Fig. 5D), yielding sensitizer enhancement ratios at 37% survival of between 2 and 3.6. The radiosensitizing effect of the combination was significantly greater in GSC than in bulk cells when SER 0.37 values were compared (Fig. 5D). Of note, R10 GSC were not radiosensitized by olaparib alone; however, combined ATR and PARP inhibition resulted in potent radiosensitization. γH2AX foci analyses confirmed that CAiPi generates an excess of DNA DSBs in GSC in combination with radiation (Fig. 5D, 5iv).

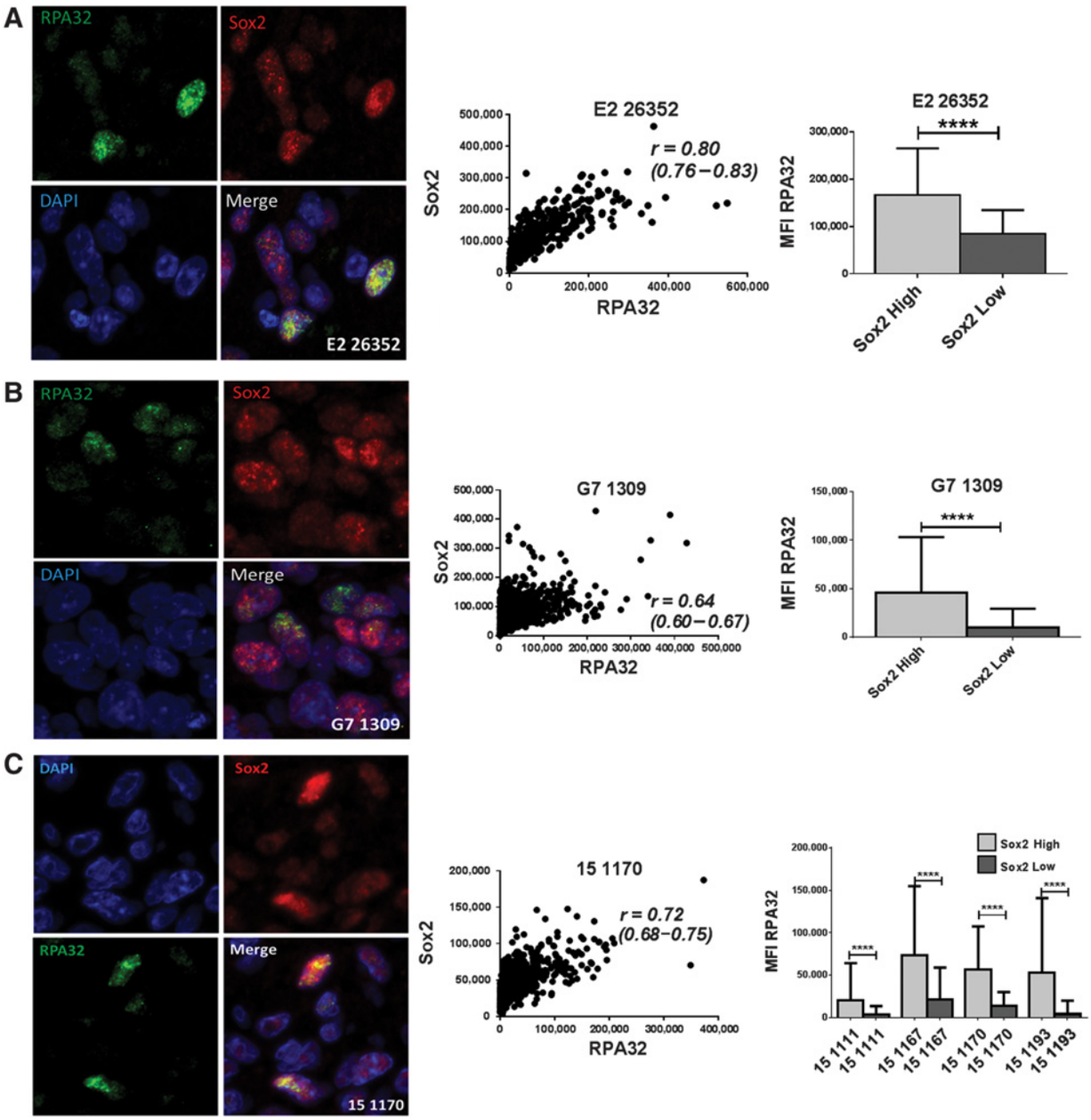

Figure 4.

GSC show enhanced RS in murine intracranial orthotopic xenografts and in human GBM tumor samples. **A** and **B,** Representative images (magnification, ×63) of immunofluorescent staining for RPA32 and Sox2 in sections from murine orthotopic intracranial xenografts derived from E2 CD133$^+$ cells (**A**) and G7 GSC cultures (**B**). Scatter plots showing correlation between Sox2 and RPA32 MFI, with corresponding *r* values (95% CI). Bar charts show RPA32 MFI quantified in Sox2-low and Sox2-high populations (defined as below and above median Sox2 MFI intensity values, respectively; mean ± SEM; unpaired *t* test). **C,** Representative images (magnification, ×63) of immunofluorescent staining for RPA32 and Sox2 in a section from a resected human GBM tumor "15 1170." Scatter plot showing correlation between Sox2 and RPA32 MFI, with corresponding *r* value (95% CI). Bar chart shows RPA32 MFI quantified in Sox2-low and Sox2-high populations (defined as above and below median Sox2 MFI values, respectively; mean ± SEM, unpaired *t* test) in four different resected human GBM specimens. ****, $P \leq 0.0001$.

Discussion

Radiation resistance of GSC is a well-recognized yet poorly understood phenomenon, comprehension of which is vitally important to attempts to improve the therapeutic index of current therapy for GBM, because improvements in patient survival depend upon our ability to control or eradicate this tumor cell fraction. Despite characterization of upregulated DDR in cancer stem cells of different tumor types, the underlying reason for activated DDR and consequent radiation resistance in GSC has remained elusive. Given the ubiquity of this phenotype in GSC

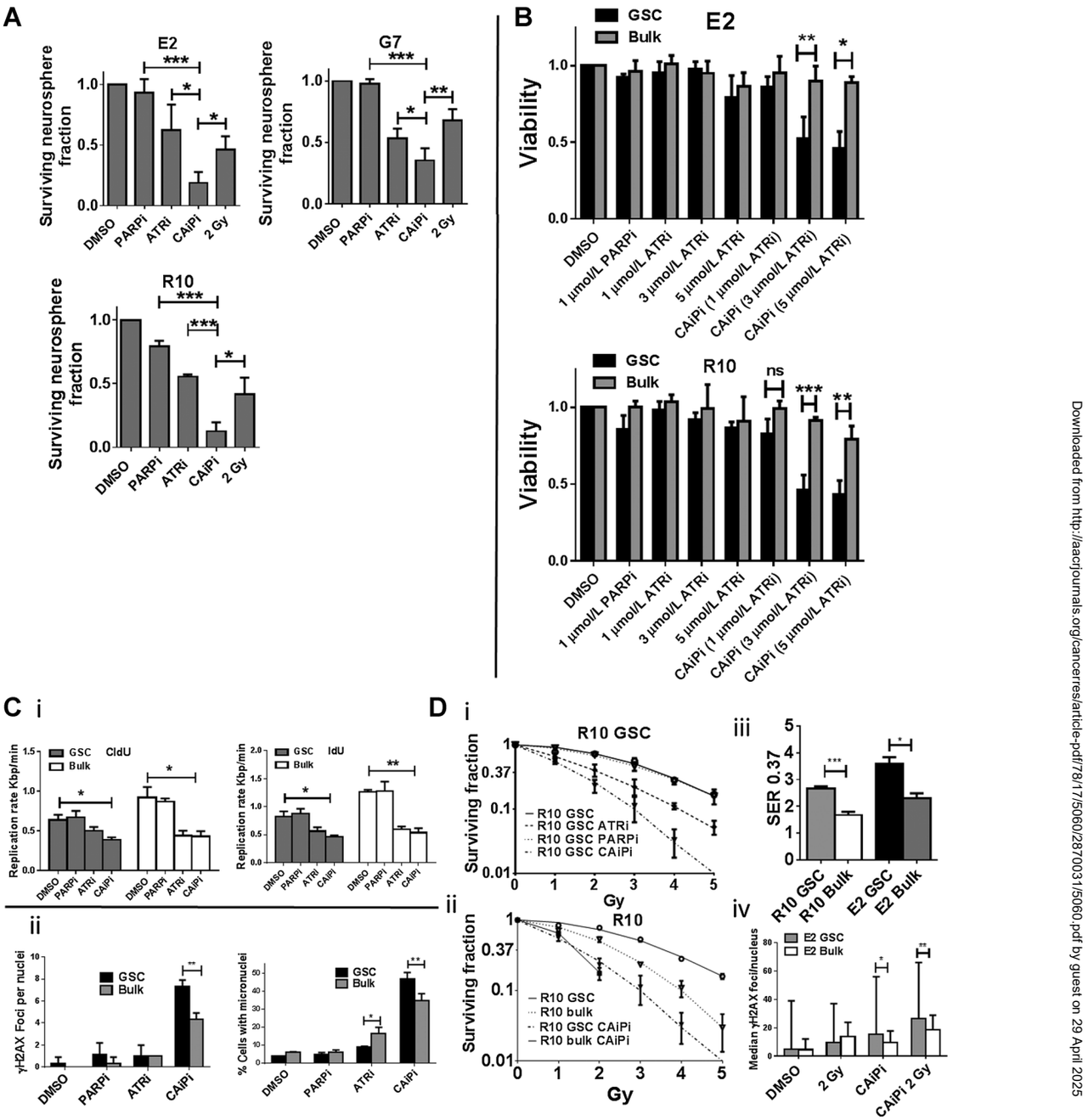

Figure 5.

Inhibition of RS response inhibits GSC neurosphere formation, generates DNA DSBs, and abrogates GSC radiation resistance. **A,** Neurosphere formation by E2, G7, and R10 GSCs following 48 hours of exposure to PARPi (1 μmol/L) or ATRi (5 μmol/L) alone, CAiPi or radiation (2 Gy). Surviving neurosphere fraction is plotted relative to DMSO control (mean ± SEM, $n = 3$; *, $P < 0.05$; **, $P < 0.01$; ***, $P < 0.001$, unpaired t test). **B,** Cell viability of paired E2 and R10 GSC and tumor bulk cultures following 24 hours of incubation with PARPi alone (1 μmol/L), incremental concentrations of ATRi alone (1, 3, and 5 μmol/L) or CAiPi. (mean ± SEM, $n = 3$; ***, $P < 0.001$; unpaired t test). **Ci,** Quantification of CldU and IdU incorporation rates (replication velocities) in E2 GSC and bulk following 24 hours of exposure to PARPi (1 μmol/L) or ATRi (5 μmol/L) alone or CAiPi as measured by DNA fiber assay (mean ± SEM, $n = 3$; unpaired t test). **ii,** Quantification of mean γH2AX foci per nuclei and micronuclei formation in E2 GSC and tumor bulk cells following 48 hours of exposure to ATRi or PARPi alone or CAiPi relative to DMSO control (mean ± SEM, $n = 3$; **, $P < 0.01$; unpaired t test). **Di,** Clonogenic survival curves derived from R10 GSC following exposure to DMSO, ATRi, PARPi, or CAiPi for 1 hour before and 24 hours after ionizing radiation (0–5 Gy; mean ± SEM, $n = 3$). **ii,** Clonogenic survival curve derived from R10 GSC and paired R10 bulk following treatment with DMSO or combined ATRi and PARPi with radiation. **iii,** Quantification of radiation sensitizer enhancement ratios for 0.37 survival following combined ATRi/PARPi in E2 and R10 GSC and bulk ($n \geq 3$, mean ± SEM). **iv,** Quantification of median γH2AX foci per nucleus in E2 GSC and bulk cells following exposure to CAiPi or DMSO for 1 hour before and 24 hours after irradiation with 2 Gy or sham irradiation. (median ± range, $n = 1$; *, $P < 0.05$; **, $P < 0.01$; Mann–Whitney U test).

and its prevalence in cancer stem cells of other tumor types, deeper understanding of the responsible mechanisms is predicted to generate highly appealing targets for clinical therapy.

RS has previously been implicated in the evolution of GBM and other cancers, particularly with regard to oncogene-induced senescence and as an anticancer barrier in early tumorigenesis (14, 47–49). Indeed, a recent study has suggested reliance upon the BRCA1–RRM2 axis for protection from RS in GBM (50). These studies validate that RS is a general feature of GBM and may result in activated DDR in the tumor as a whole; however, they do not address whether RS is of particular importance in GSC or the role of RS in determining DDR activation in GSC and have not shown that RS is responsible for radiation resistance. RS has recently been documented in nonmalignant embryonic stem cells, which display constitutively active DDR and prolonged S-phase occupancy due to abnormal cell-cycle progression. These features rapidly diminish upon differentiation (9). Our data provide novel insights into the importance of RS in the GSC phenotype and direct evidence that RS is responsible for the activation of DDR and subsequent radiation resistance in GSC.

Furthermore, we identify replication–transcription collisions as a result of increased expression of long neural genes as a likely mechanism for RS in GSC, an observation that correlates closely with recently published studies in neural progenitor cells that demonstrate that DSB arising from replication stress are preferentially located in long neural genes (20). Indeed, several of these genes, namely, *DCC, CADM2*, and *PTPRT*, are significantly overexpressed across a panel of 7 GSC cultures. A further study of particular relevance to our data has recently described a novel mechanism for oncogenic RS dependent upon intragenic origin firing within highly transcribed genes (43). Taken together, these data support the controversial hypothesis that GSC derive from neural stem cells and provide grounds for further studies.

Finally, we show that RS responses in GSC can be specifically targeted via dual inhibition of the key DDR and RS response proteins PARP and ATR. Our data demonstrate that GSC are significantly more sensitive to RS response targeting than non-GSC because of increased DNA DSB formation in GSC. Interestingly, GSC were also sensitized to radiation by dual ATR–PARP inhibition to a significantly greater degree than non-GSC, further validating our hypothesis that the radiation resistance of GSC is highly dependent on RS. Our results also suggest the feasibility of DDR targeting agents as promising therapies for GBM, both alone and in combination with radiotherapy.

Overall, our observations elucidate for the first time the mechanism underlying DDR activation and radioresistance in GSC, support an NSC origin for GSC, and identify RS response as a GSC-specific therapeutic target with the potential to improve patient outcomes from GBM.

Disclosure of Potential Conflicts of Interest

A.J. Chalmers reports receiving a commercial research grant from AstraZeneca and Vertex Pharmaceuticals, has received honoraria from the speakers bureau of Bayer, is a consultant/advisory board member for AstraZeneca and Vertex Pharmaceuticals. No potential conflicts of interest were disclosed by the other authors.

Authors' Contributions

Conception and design: R.D. Carruthers, S.U. Ahmed, A.J. Chalmers
Development of methodology: R.D. Carruthers, S.U. Ahmed, K. Strathdee, N. Gomez-Roman, A.J. Chalmers
Acquisition of data (provided animals, acquired and managed patients, provided facilities, etc.): R.D. Carruthers, S.U. Ahmed, S. Ramachandran, K. Strathdee, K.M. Kurian, N. Gomez-Roman, L. Gilmour, A.J. Chalmers
Analysis and interpretation of data (e.g., statistical analysis, biostatistics, computational analysis): R.D. Carruthers, S.U. Ahmed, S. Ramachandran, K. Strathdee, K.M. Kurian, A. Hedley, N. Gomez-Roman, M. Neilson, E.M. Hammond, A.J. Chalmers
Writing, review, and/or revision of the manuscript: R.D. Carruthers, S.U. Ahmed, K. Strathdee, K.M. Kurian, N. Gomez-Roman, E.M. Hammond, A.J. Chalmers
Administrative, technical, or material support (i.e., reporting or organizing data, constructing databases): R.D. Carruthers, K. Strathdee, K.H. Stevenson
Study supervision: A.J. Chalmers

Acknowledgments

R. Carruthers and K. Strathdee are funded by a Cancer Research UK Clinician Scientist Fellowship Award (23920) awarded to R. Carruthers. R. Carruthers was also funded by a Beatson Cancer Charity Clinical Research Fellow award. E. Hammond and S. Ramachandran are funded by a Cancer Research UK grant (C5255/A23755) awarded to E Hammond.

The costs of publication of this article were defrayed in part by the payment of page charges. This article must therefore be hereby marked *advertisement* in accordance with 18 U.S.C. Section 1734 solely to indicate this fact.

Received February 23, 2018; revised May 25, 2018; accepted June 28, 2018; published first July 5, 2018.

References

1. Parsons DW, Jones S, Zhang X, Lin JC, Leary RJ, Angenendt P, et al. An integrated genomic analysis of human glioblastoma multiforme. Science 2008;321:1807–12.
2. Ajaz M, Jefferies S, Brazil L, Watts C, Chalmers A. Current and investigational drug strategies for glioblastoma. Clin Oncol (R Coll Radiol) 2014;26:419–30.
3. Stupp R, Mason WP, van den Bent MJ, Weller M, Fisher B, Taphoorn MJ, et al. Radiotherapy plus concomitant and adjuvant temozolomide for glioblastoma. N Engl J Med 2005;352:987–96.
4. Bao S, Wu Q, McLendon RE, Hao Y, Shi Q, Hjelmeland AB, et al. Glioma stem cells promote radioresistance by preferential activation of the DNA damage response. Nature 2006;444:756–60.
5. Chen J, Li Y, Yu TS, McKay RM, Burns DK, Kernie SG, et al. A restricted cell population propagates glioblastoma growth after chemotherapy. Nature 2012;488:522–6.
6. Auffinger B, Tobias AL, Han Y, Lee G, Guo D, Dey M, et al. Conversion of differentiated cancer cells into cancer stem-like cells in a glioblastoma model after primary chemotherapy. Cell Death Differ 2014;21:1119–31.
7. Eyler CE, Rich JN. Survival of the fittest: cancer stem cells in therapeutic resistance and angiogenesis. J Clin Oncol 2008;26:2839–45.
8. Desai A, Webb B, Gerson SL. $CD133^+$ cells contribute to radioresistance via altered regulation of DNA repair genes in human lung cancer cells. Radiother Oncol 2014;110:538–45.
9. Ahuja AK, Jodkowska K, Teloni F, Bizard AH, Zellweger R, Herrador R, et al. A short G1 phase imposes constitutive replication stress and fork remodelling in mouse embryonic stem cells. Nat Commun. 2016; 7:10660.
10. Venere M, Hamerlik P, Wu Q, Rasmussen RD, Song LA, Vasanji A, et al. Therapeutic targeting of constitutive PARP activation compromises stem cell phenotype and survival of glioblastoma-initiating cells. Cell Death Differ 2014;21:258–69.
11. Diehn M, Cho RW, Lobo NA, Kalisky T, Dorie MJ, Kulp AN, et al. Association of reactive oxygen species levels and radioresistance in cancer stem cells. Nature 2009;458:780–3.
12. Ahmed SU, Carruthers R, Gilmour L, Yildirim S, Watts C, Chalmers AJ. Selective Inhibition of Parallel DNA Damage Response Pathways

Optimizes Radiosensitization of Glioblastoma Stem-like Cells. Cancer Res 2015;75:4416–28.
13. Biddlestone-Thorpe L, Sajjad M, Rosenberg E, Beckta JM, Valerie NC, Tokarz M, et al. ATM kinase inhibition preferentially sensitizes p53-mutant glioma to ionizing radiation. Clin Cancer Res 2013;19:3189–200.
14. Bartkova J, Hamerlik P, Stockhausen MT, Ehrmann J, Hlobilkova A, Laursen H, et al. Replication stress and oxidative damage contribute to aberrant constitutive activation of DNA damage signalling in human gliomas. Oncogene 2010;29:5095–102.
15. Olcina MM, Foskolou IP, Anbalagan S, Senra JM, Pires IM, Jiang Y, et al. Replication stress and chromatin context link ATM activation to a role in DNA replication. Mol Cell 2013;52:758–66.
16. Zeman MK, Cimprich KA. Causes and consequences of replication stress. Nat Cell Biol 2014;16:2–9.
17. Foskolou IP, Jorgensen C, Leszczynska KB, Olcina MM, Tarhonskaya H, Haisma B, et al. Ribonucleotide reductase requires subunit switching in hypoxia to maintain DNA replication. Mol Cell 2017;66:206–20 e9.
18. Kim JK, Jeon HM, Jeon HY, Oh SY, Kim EJ, Jin X, et al. Conversion of glioma cells to glioma stem-like cells by angiocrine factors. Biochem Biophys Res Commun. 2017.
19. Alcantara Llaguno SR, Wang Z, Sun D, Chen J, Xu J, Kim E, et al. Adult lineage-restricted CNS progenitors specify distinct glioblastoma subtypes. Cancer Cell 2015;28:429–40.
20. Wei PC, Chang AN, Kao J, Du Z, Meyers RM, Alt FW, et al. Long neural genes harbor recurrent DNA break clusters in neural stem/progenitor cells. Cell 2016;164:644–55.
21. Fael Al-Mayhani TM, Ball SL, Zhao JW, Fawcett J, Ichimura K, Collins PV, et al. An efficient method for derivation and propagation of glioblastoma cell lines that conserves the molecular profile of their original tumours. J Neurosci Methods 2009;176:192–9.
22. Gomez-Roman N, Stevenson K, Gilmour L, Hamilton G, Chalmers AJ. A novel 3D human glioblastoma cell culture system for modeling drug and radiation responses. Neuro Oncol. 2016;19:229–41.
23. Carruthers R, Ahmed SU, Strathdee K, Gomez-Roman N, Amoah-Buahin E, Watts C, et al. Abrogation of radioresistance in glioblastoma stem-like cells by inhibition of ATM kinase. Mol Oncol 2015;9:192–203.
24. Mirzoeva OK, Petrini JHJ. DNA damage-dependent nuclear dynamics of the Mre11 complex. Mol Cell Biol 2001;21:281–8.
25. Church DM, Schneider VA, Graves T, Auger K, Cunningham F, Bouk N, et al. Modernizing reference genome assemblies. PLoS Biol 2011;9: e1001091.
26. Kim D, Pertea G, Trapnell C, Pimentel H, Kelley R, Salzberg SL. TopHat2: accurate alignment of transcriptomes in the presence of insertions, deletions and gene fusions. Genome Biol 2013;14:R36.
27. Langmead B, Trapnell C, Pop M, Salzberg SL. Ultrafast and memory-efficient alignment of short DNA sequences to the human genome. Genome Biol 2009;10:R25.
28. Anders S, Huber W. Differential expression analysis for sequence count data. Genome Biol 2010;11:R106.
29. Mannino M, Gomez-Roman N, Hochegger H, Chalmers AJ. Differential sensitivity of Glioma stem cells to Aurora kinase A inhibitors: implications for stem cell mitosis and centrosome dynamics. Stem Cell Res 2014; 13:135–43.
30. Zou L, Elledge SJ. Sensing DNA damage through ATRIP recognition of RPA-ssDNA complexes. Science 2003;300:1542–8.
31. Liu S, Opiyo SO, Manthey K, Glanzer JG, Ashley AK, Amerin C, et al. Distinct roles for DNA-PK, ATM and ATR in RPA phosphorylation and checkpoint activation in response to replication stress. Nucleic Acids Res 2012;40:10780–94.
32. Gagou ME, Zuazua-Villar P, Meuth M. Enhanced H2AX phosphorylation, DNA replication fork arrest, and cell death in the absence of Chk1. Mol Biol Cell 2010;21:739–52.
33. Marti TM, Hefner E, Feeney L, Natale V, Cleaver JE. H2AX phosphorylation within the G1 phase after UV irradiation depends on nucleotide excision repair and not DNA double-strand breaks. Proc Natl Acad Sci U S A 2006;103:9891–6.
34. Vesela E, Chroma K, Turi Z, Mistrik M. Common chemical inductors of replication stress: focus on cell-based studies. Biomolecules. 2017;7.
35. Helmrich A, Ballarino M, Tora L. Collisions between replication and transcription complexes cause common fragile site instability at the longest human genes. Mol Cell 2011;44:966–77.
36. Zhang Y, Huang L, Fu H, Smith OK, Lin CM, Utani K, et al. A replicator-specific binding protein essential for site-specific initiation of DNA replication in mammalian cells. Nat Commun. 2016;7:11748.
37. Meister P, Taddei A, Ponti A, Baldacci G, Gasser SM. Replication foci dynamics: replication patterns are modulated by S-phase checkpoint kinases in fission yeast. EMBO J 2007;26:1315–26.
38. Smith DI, Zhu Y, McAvoy S, Kuhn R. Common fragile sites, extremely large genes, neural development and cancer. Cancer Lett 2006;232: 48–57.
39. Helmrich A, Stout-Weider K, Hermann K, Schrock E, Heiden T. Common fragile sites are conserved features of human and mouse chromosomes and relate to large active genes. Genome Res 2006;16:1222–30.
40. Xu B, Goldman JS, Rymar VV, Forget C, Lo PS, Bull SJ, et al. Critical roles for the netrin receptor deleted in colorectal cancer in dopaminergic neuronal precursor migration, axon guidance, and axon arborization. Neuroscience 2010;169:932–49.
41. Lim SH, Kwon SK, Lee MK, Moon J, Jeong DG, Park E, et al. Synapse formation regulated by protein tyrosine phosphatase receptor T through interaction with cell adhesion molecules and Fyn. EMBO J 2009;28: 3564–78.
42. Frei JA, Andermatt I, Gesemann M, Stoeckli ET. The SynCAM synaptic cell adhesion molecules are involved in sensory axon pathfinding by regulating axon-axon contacts. J Cell Sci 2014;127(Pt 24):5288–302.
43. Macheret M, Halazonetis TD. Intragenic origins due to short G1 phases underlie oncogene-induced DNA replication stress. Nature 2018;555: 112–6.
44. Modrek AS, Bayin NS, Placantonakis DG. Brain stem cells as the cell of origin in glioma. World J Stem Cells 2014;6:43–52.
45. Reaper PM, Griffiths MR, Long JM, Charrier JD, Maccormick S, Charlton PA, et al. Selective killing of ATM- or p53-deficient cancer cells through inhibition of ATR. Nat Chem Biol 2011;7:428–30.
46. Bryant HE, Petermann E, Schultz N, Jemth AS, Loseva O, Issaeva N, et al. PARP is activated at stalled forks to mediate Mre11-dependent replication restart and recombination. EMBO J 2009;28:2601–15.
47. Bartkova J, Horejsi Z, Koed K, Kramer A, Tort F, Zieger K, et al. DNA damage response as a candidate anti-cancer barrier in early human tumorigenesis. Nature 2005;434:864–70.
48. Di Micco R, Fumagalli M, Cicalese A, Piccinin S, Gasparini P, Luise C, et al. Oncogene-induced senescence is a DNA damage response triggered by DNA hyper-replication. Nature 2006;444:638–42.
49. Bartkova J, Rezaei N, Liontos M, Karakaidos P, Kletsas D, Issaeva N, et al. Oncogene-induced senescence is part of the tumorigenesis barrier imposed by DNA damage checkpoints. Nature 2006;444:633–7.
50. Rasmussen RD, Gajjar MK, Tuckova L, Jensen KE, Maya-Mendoza A, Holst CB, et al. BRCA1-regulated RRM2 expression protects glioblastoma cells from endogenous replication stress and promotes tumorigenicity. Nat Commun. 2016;7:13398.